Article

Highly Conductive Mn-Co Spinel Powder Prepared by Cu-Doping Used for Interconnect Protection of SOFC

Zhou Jiang [1,2], Kui Wen [2,*], Chen Song [2], Taikai Liu [2,*], Yong Dong [1], Min Liu [2], Changguang Deng [2], Chunming Deng [2] and Chenghao Yang [3]

1 School of Materials and Energy, Guangdong University of Technology, Guangzhou 510640, China; jiangzhou_2019@163.com (Z.J.); yongdong@gdut.edu.cn (Y.D.)
2 National Engineering Laboratory for Modern Materials Surface Engineering Technology, The Key Lab of Guangdong for Modern Surface Engineering Technology, Guangdong Institute of New Materials, Guangdong Academy of Science, Guangzhou 510651, China; songchen@gdinm.com (C.S.); liumin@gdinm.com (M.L.); dengchangguang@gdinm.com (C.D.); dengchunming@gdinm.com (C.D.)
3 School of Environment and Energy, South China University of Technology, Guangzhou 510006, China; esyangc@scut.edu.cn
* Correspondence: wenkui@gdinm.com (K.W.); liutaikai@gdinm.com (T.L.)

Abstract: Mn-Co Spinel is considered as one of the most promising materials for the interconnect protection of solid oxide fuel cells; however, its conductivity is too low to maintain a high cell performance as compared with cathode materials. Element doping is an effective method to improve the spinel conductivity. In this work, we proposed doping Mn-Co spinel powder with Cu via a solid phase reaction. $Cu_\delta Mn_{1.5-x}Co_{1.5-y}O_4$ with δ = 0.1, 0.2, 0.3, and x + y = δ was obtained. X-ray diffraction (XRD) and thermogravimetry-differential scanning calorimetry (TG-DSC) were used to evaluate the Cu-doping effect. After sintering at 1000 °C for 12 h, the yield exhibited the best crystallinity, density, and element distribution, with a phase composition of $MnCo_2O_4/Cu_xMn_{3-x}O_4$ (x = 1, 1.2, 1.4 or 1.5). X-ray photoelectron spectroscopy (XPS) was used to semi-quantitatively characterize the content changes in element valence states. The areal fraction of Mn^{2+} and Co^{3+} was found to decrease when the sintering duration increased, which was attributed to the decomposition of the $MnCo_2O_4$ phase. Finally, coatings were prepared by atmospheric plasma spraying with doped spinel powders and the raw powder $Mn_{1.5}Co_{1.5}O_4$. It was found that Cu doping can effectively increase the conductivity of Mn-Co spinel coatings from 23 S/cm to 51 S/cm. Although the dopant Cu was found to be enriched on the surface of the coatings after the conductivity measurement, which restrained the doping effect, Cu doping remains a convenient method to significantly promote the conductivity of spinel coatings for SOFC applications.

Keywords: Mn-Co spinel; Cu doping; conductivity; SOFC; interconnect

1. Introduction

Solid oxide fuel cells (SOFC) are high-temperature energy conversion devices that can directly convert the chemical energy of fuel into electrical energy. They mainly consist of a porous anode/cathode, a dense electrolyte, and an interconnect. As an important part, the interconnect provides electrical contact between cells while isolating fuel gas from air. Ferritic stainless steel (FSS) has been widely used as interconnect material due to its outstanding oxidation resistance and suitable thermal expansion coefficient [1–3]. However, at elevated temperature, the Cr of FSS is oxidized to form Cr_2O_3, CrO_3, or even $CrO_2(OH)_2$. These substances can accumulate at the cathode and react with cathode materials, forming a low active phase and deteriorating cell performance. At present, the above problems are mainly solved by introducing protective coatings [4,5].

$(Mn,Co)_3O_4$ spinel coating is often used to diminish the evaporation of Cr and thus reduce the performance degradation and prolong the service life of the stack. However,

the theoretical conductivity of $(Mn,Co)_3O_4$ spinel at elevated temperature is only 60 S/cm, which is much lower than that of the cathode material, such as LSCF > 200 S/cm at 600–800 °C [6–9]. Many efforts have been made to improve the conductivity of Mn-Co spinel coating. Fe doping can reduce the growth of Cr_2O_3 film and improve the oxidation resistance, but this reduces the conductivity of spinel coatings [10–13]. Ce doping can enhance the adhesion and improve the interfacial stability of oxide film, but the effects depend on the substrate materials [14–16]. Cu doping can improve the conductivity and adjust the thermal expansion coefficient of spinel coatings [17–19].

For promoting the conductivity of Mn-Co spinel coatings, in this work, we prepared Cu-doped Mn-Co spinel powder via the solid-phase reaction method. The doped powder was denoted as $Cu_\delta Mn_{1.5-x}Co_{1.5-y}O_4$ (δ = 0.1, 0.2, 0.3, x + y = δ). The first part of this work was to study the optimal doping amount of Cu, and then the doping conditions were studied to improve the doping effect. Finally, the doped powder was used to prepare coatings on FSS substrate to evaluate the doping effect using a plasma spray.

2. Experiment

2.1. Powder Preparation and Characterization

The raw materials, as shown in Figure 1, were Cu powders (Tijo, Changsha, China) with D_{50} = 21.58 μm, and $Mn_{1.5}Co_{1.5}O_4$ powder with D_{50} = 19.2 μm (Terio, Qingdao, China). Three groups of doping powder were prepared with controlled Cu-doping as shown in Table 1. The raw powders were mechanically mixed in a roller mixer at a speed of 600 r/min for 20 h. After mixing, the powders were transferred into a muff furnace for solid-phase reaction sintering, and then the sintered powders were sieved to maintain the particle size below 50 μm. The phase structure of the sieved powders was checked by X-ray diffraction (XRD, Bruker D8 Advance, Bruker Cop., Karlsruhe, Germany) in the range of 10–90° (0.01°/step, 0.167 s/step). The micromorphology and element distribution of the sieved powders were characterized by a scanning electron microscope (SEM, Nova-Nano-450, FEI, Hillsboro, OR, USA) and energy dispersive spectrometer (EDS, XLT TEM-SDD, AMETEK EDAX, Philadelphia, PA, USA). The solid-phase sintering process was investigated using a thermogravimetry-differential scanning calorimetry (TG-DSC, STA-449-F5, NETZSCH, Selb, Germany) test with a heating rate of 5 °C/min in air. The valence states of the sintered powders were analyzed by X-ray photoelectron spectroscopy (XPS, Thermo Fisher Scientific Nexsa, Thermo Fisher Scientific Inc., Waltham, MA, USA), and then the content changes in the element valence states were characterized semi-quantitatively. The XPS spectra were obtained with monochromatized Al Kα radiation. All spectra were recorded at a take-off angle of 90°. The carbon C 1s peak with a binding energy of 284.5 eV was used for calibration.
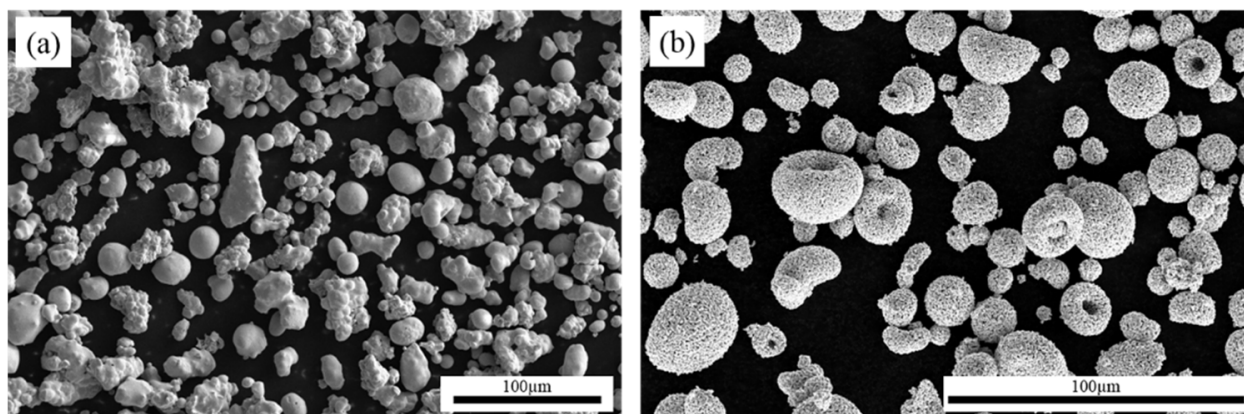

Figure 1. The morphology of Cu powder (**a**) and $Mn_{1.5}Co_{1.5}O_4$ powder (**b**).

Table 1. The raw material ratio to prepare $Cu_\delta Mn_{1.5-x}Co_{1.5-y}O_4$ powders.

| Mass Percentage (wt%)	$\delta = 0.1$	$\delta = 0.2$	$\delta = 0.3$
Cu Powder	2.7	5.4	8.0
$Mn_{1.5}Co_{1.5}O_4$ Power	97.3	94.6	92.0

2.2. Coating Preparation

Al_2O_3 sheets (φ 18.55 mm $\times$ 1.65 mm) were used as substrates. $Mn_{1.5}Co_{1.5}O_4$ and doped $Cu_{0.3}Mn_{1.5-x}Co_{1.5-y}O_4$ powders were used as spraying feedstocks. Atmospheric plasma spraying equipment (model CLWI-091, GTV, Luckenbach, Germany) was used to prepare the spinel coating. The spraying process parameters are shown in Table 2. Before spraying, substrates were ultrasonically cleaned with alcohol to remove any oil and impurities on the surface.

Table 2. Spray parameters to prepare Cu-doped Mn-Co spinel coatings.

Gas Flow (NL/min)		Current (A)	Gun Speed (mm/s)	Powder Feeding Rate (g/min)	Spray Distance (mm)
Ar/72	H_2/8	620	800	15	110

2.3. Coating Characterization

The sectional morphology, density, and element distribution of the spinel coating were analyzed by SEM and EDS. The phase composition of the coating was characterized by XRD. The conductivity of coatings was determined by the four-probe method. The conductivity test setup is shown in Figure 2. Testing samples were placed in a tubular furnace, which was heated up to 800 °C at a rate of 5 °C/min. A constant current of 0.2 A was provided between I^+ and I^- through silver lines, and the corresponding voltage between U^+ and U^- was recorded. The coating conductivity (ε, S/cm) was obtained as $\varepsilon = 1 \div (C \times R \times W)$, where C denotes the wiring coefficient, R denotes the calculated resistance (Ω), and W denotes the thickness of the coating (cm).
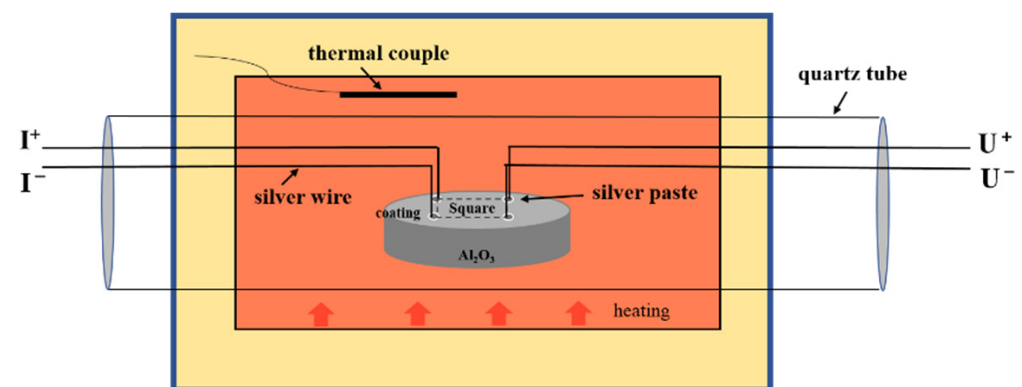

Figure 2. Illustration of the conductivity measurements setup.

3. Results and Discussion

3.1. Phases and Structures

Figure 3 shows the XRD patterns of $Cu_\delta Mn_{1.5-x}Co_{1.5-y}O_4$ ($\delta = 0$, 0.1, 0.2, 0.3, x + y = δ) powders sintered at 900 °C for 12 h. $Cu_\delta Mn_{1.5-x}Co_{1.5-y}O_4$ ($\delta = 0.1$, 0.2, 0.3) powders were composed of CuO, $MnCo_2O_4$, $Cu_xMn_{3-x}O_4$ (x = 1, 1.2, 1.4, or 1.5), and $(Co,Mn)(Co,Mn)_2O_4$. $(Co,Mn)(Co,Mn)_2O_4$ is a mixture of $MnCo_2O_4$ and $CoMn_2O_4$. Cu-doping can promote the formation of the cubic spinel phase. After increasing the amount of Cu-doping, the diffraction peaks were found to shift slightly toward the right because of the replacement of Co^{2+} (0.074 nm) with Cu^{2+} (0.073 nm), and the diffraction intensity of $(Co,Mn)(Co,Mn)_2O_4$ and CuO was found to decrease, which indicates the doping reactions had taken place.

When both CuO and CoMn$_2$O$_4$ were present in the coating, the uniformity and conductivity of the powder were reduced [18]. It was found that the (Co,Mn)(Co,Mn)$_2$O$_4$ and CuO of Cu$_{0.3}$Mn$_{1.5-x}$Co$_{1.5-y}$O$_4$ powder exhibited the lowest diffraction intensity and the best crystallinity of the spinel phase.
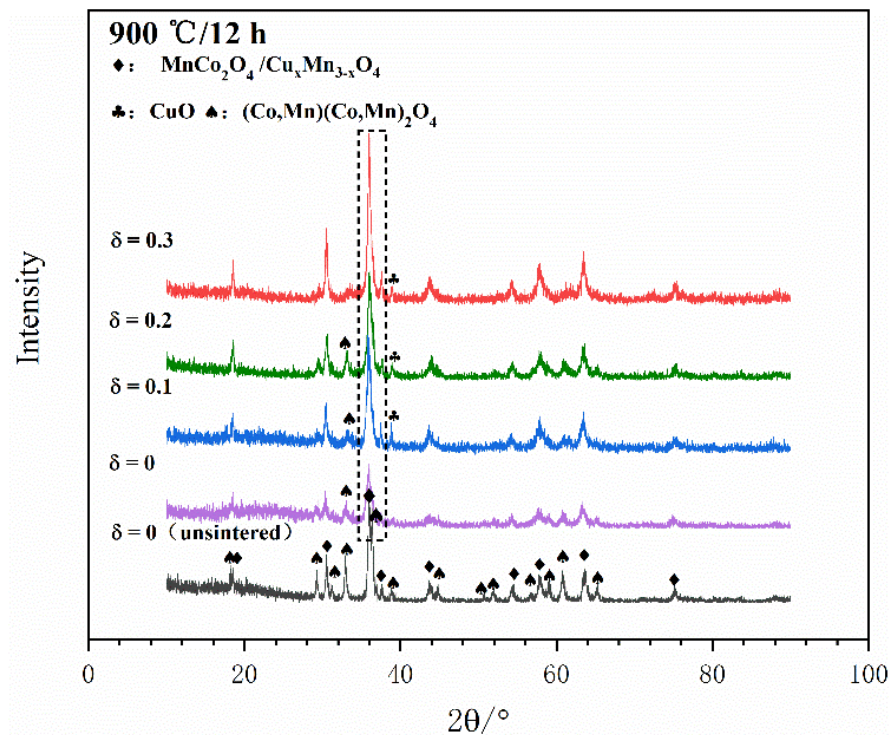

Figure 3. XRD patterns of Mn$_{1.5}$Co$_{1.5}$O$_4$ powder and Cu$_\delta$Mn$_{1.5-0.5x}$Co$_{1.5-0.5x}$O$_4$ powder.

3.2. Solid Phase Reactions

Cu$_\delta$Mn$_{1.5-x}$Co$_{1.5-y}$O$_4$ (δ = 0, 0.1, 0.2, 0.3) powders were tested by TG-DSC to evaluate the physical and chemical changes during sintering. According to the TG curve in Figure 4a and the subsequent XRD analysis (Figure 5), it was found that the powders gained some weight at 500–800 °C, which was mainly attributed to the oxidization of Cu to CuO. However, at 800–1000 °C, the powder weights were found to decrease slightly and the CuO had disappeared. At 1034 °C, the powder weight was slightly decreased again, which might be related to the decomposition of the spinel phase. Then, the powder was found to lose weight violently between 1200–1300 °C, which indicates that the spinel phases were decomposed. As shown in Figure 4b, the commercial Mn$_{1.5}$Co$_{1.5}$O$_4$ powder had no endothermic peak at 1034 °C, while Cu$_\delta$Mn$_{1.5-x}$Co$_{1.5-y}$O$_4$ (δ = 0.1, 0.2, 0.3) powder had an endothermic peak. According to public reports [9,13,20,21], the formation of Cu$_x$Mn$_{3-x}$O$_4$ and MnCo$_2$O$_4$ is an exothermic process. Since the MnCo$_2$O$_4$ phase of the commercial Mn$_{1.5}$Co$_{1.5}$O$_4$ powder showed no significant decomposition at 1034 °C, it was inferred that the endothermic peak at 1034 °C was the result of the decomposition of Cu$_x$Mn$_{3-x}$O$_4$. Furthermore, in the range 1100–1300 °C, after increasing the amount of Cu, the TG curve shifted toward the left, and the stable temperature of the spinel phases decreased. The DSC curves were found to gradually flatten and continuously exhausted heat. As shown in Figure 4c,d, the Cu$_{0.3}$Mn$_{1.5-x}$Co$_{1.5-y}$O$_4$ powder exhibited the best crystallization. In conclusion, Cu$_x$Mn$_{3-x}$O$_4$ spinel was successfully synthesized between 900 °C and 1034 °C. The powders with δ = 0.3 had the best crystallinity of spinel phases and consisted of more conductive spinel phase.
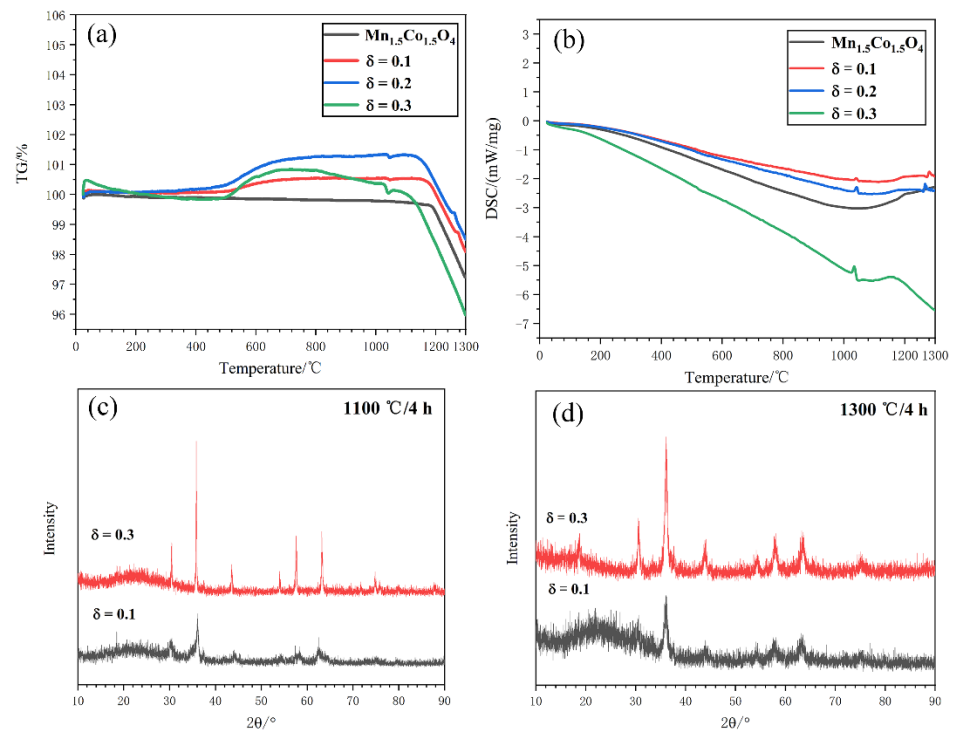
Figure 4. (**a**) TG curves of $Cu_\delta Mn_{1.5-x}Co_{1.5-y}O_4$ powders; (**b**) DSC curve; (**c**) XRD patterns of powder sintered at 1100 °C for 4 h with δ = 0.1 and 0.3; (**d**) XRD patterns of powder sintered at 1300 °C for 4 h with δ = 0.1 and 0.3.
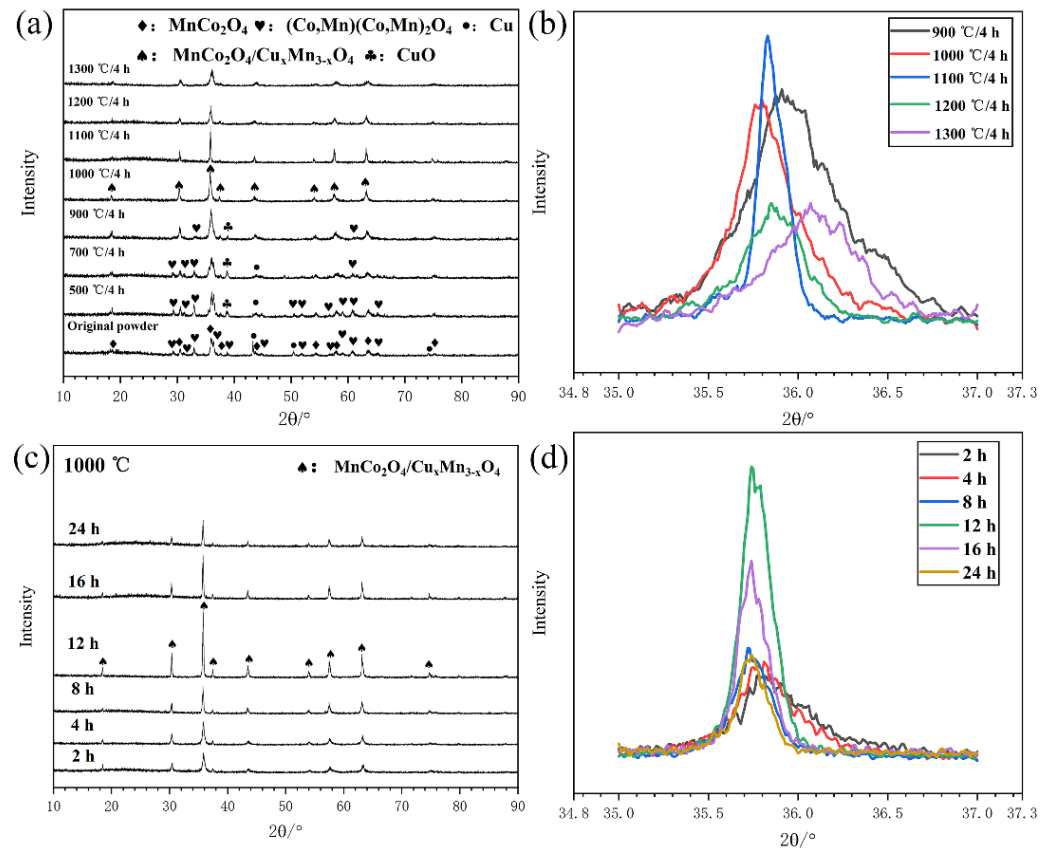
Figure 5. XRD patterns of doped powders sintered under different conditions: (**a**,**b**) 500–1300 °C for 4 h; (**c**,**d**) 1000 °C for 2–24 h.

3.3. Sintering Conditions

$Cu_{0.3}Mn_{1.5-x}Co_{1.5-y}O_4$ powders were prepared at controlled sintering temperatures and durations. Cu was introduced into the spinel lattice by sintering. The more Cu that entered the spinel lattice, the better the conductivity of the coating. The phase composition, crystallization, and surface morphology of the prepared $Cu_{0.3}Mn_{1.5-x}Co_{1.5-y}O_4$ powders were specifically investigated. According to the XRD patterns of the powders sintered at 500–1300 °C for 4 h, it was found that, with the increase in sintering temperature, the abundance of CuO and $(Co,Mn)(Co,Mn)_2O_4$ phases reduced, while the abundance of $MnCo_2O_4/Cu_xMn_{3-x}O_4$ spinel phases increased. The crystallinity of the spinel phases increased firstly and then decreased as the temperature increased; thus, the best crystallization temperature was between 1000–1100 °C, as shown in Figure 5. According to the morphology of the sintered powders, the powder density was found to increase when the temperature increased from 900 °C to 1300 °C. After sintering between 1100–1300 °C, the powder was found to be severely agglomerated, as shown in Figure 6, while at 1000 °C, the powder porosity was reduced.
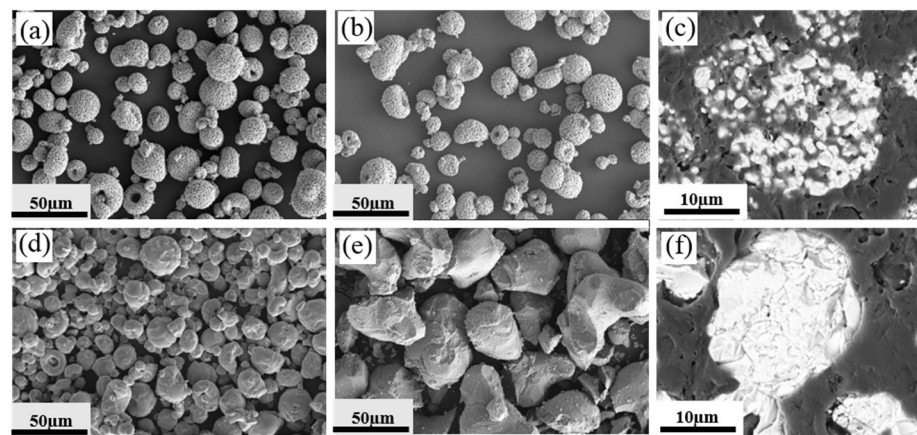
Figure 6. The morphology of $Cu_{0.3}Mn_{1.5-x}Co_{1.5-y}O_4$ powders sintered at: (**a**) 900 °C for 12 h; (**b**) 1000 °C for 12 h; (**c**) 1000 °C for 12 h (cross-sectional); (**d**) 1100 °C for 4 h; (**e**) 1300 °C for 4 h; (**f**) 1100 °C for 4 h (cross-sectional).

After sintering at 1000 °C for 2 h, 4 h, 8 h, 12 h, 16 h, and 24 h, the intensity of the diffraction peak and crystallinity of spinel were found to firstly increase and then decrease after 12 h. The change in diffraction peaks was related to the amount of spinel phases. The diffraction intensity of powder sintered for 12 h was the highest and the crystallinity was the best, as shown in Figure 5c,d. In Figure 7, EDS analysis showed a uniform distribution of Cu, which indicates that the Cu has been sucessfully doped into $Mn_{1.5}Co_{1.5}O_4$ spinel powders. In conclusion, 1000 °C/12 h was the best condition for Cu doping.
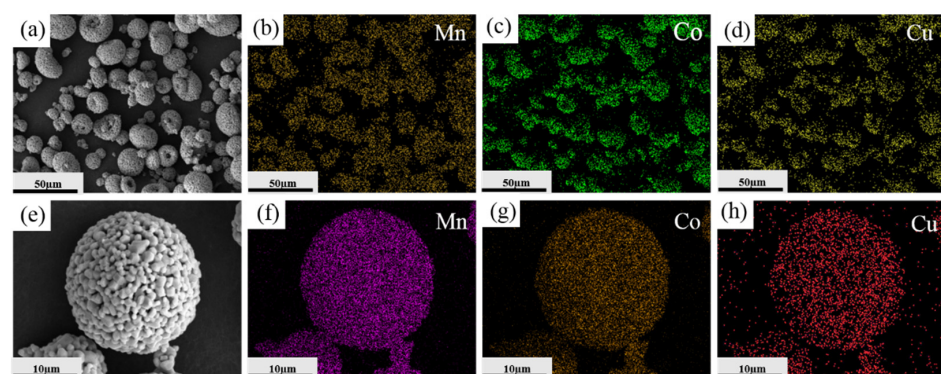
Figure 7. The morphology and elements distribution of $Cu_{0.3}Mn_{1.5-x}Co_{1.5-y}O_4$ powders sintered at 1000 °C for 12 h (**a–d**) low magnification; (**e–h**) high magnification.

3.4. Stability of Doped Powders

As Cu-Mn spinel is less stable than Mn-Co spinel at elevated temperature, when doping Mn-Co spinel with Cu to improve the conductivity, the stability of the obtained spinel is reduced. After being sintered at 1000 °C for 4 h, 12 h, and 24 h to allow the doping, the $Cu_{0.3}Mn_{1.5-x}Co_{1.5-y}O_4$ powder was heated to 800 °C and maintained in that state for 12 h to evaluate the stability. In Figure 8a, the XRD patterns before and after the heat treatment are presented. The $MnCo_2O_4/Cu_xMn_{3-x}O_4$ phase was detected after the heat treatment, but the diffraction intensity was significantly diminished. TG and DSC tests were performed from room temperature to 800 °C with a ramping rate of 5 °C/min, and a preservation stage of 12 h, in order to study the stability of the doped powders. It was found that during ramping, the DSC plots showed evident exothermic behavior. However, during the following preservation stage, both the TG and DSC curves exhibited a linear behavior in which no endothermic and exothermic peak was visible, as shown in Figure 8b–d. This indicates that the doped powder had a good stability during the preservation process. For the $Cu_xMn_{3-x}O_4$ powder, when x = 1.2, 1.4, 1.5, the CuO and spinel phase coexisted at 800 °C. However, according to the XRD and DSC patterns, it can be seen that the decomposition of $Cu_xMn_{3-x}O_4$ spinel did not occur and CuO was not formed. Therefore, the $Cu_xMn_{3-x}O_4$ phase was mainly composed of the $CuMn_2O_4$ phase. In conclusion, the $MnCo_2O_4/CuMn_2O_4$ phase in the powder can exist stably at 800 °C.
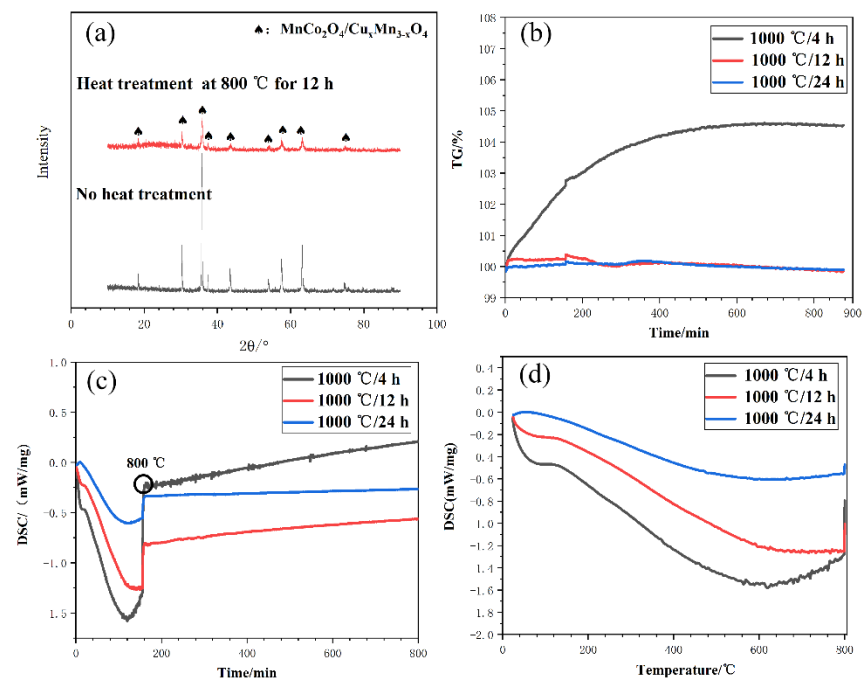

Figure 8. (**a**) XRD patterns before and after heating at 800 °C of powder sintered at 1000 °C for 12 h; (**b**,**c**) TG-DSC curves of powders sintered at 1000 °C for 4 h, 12 h, and 24 h; (**d**) DSC curves during the heating process.

3.5. Elemental Composition

To determine the elemental composition and valence states of $Cu_{0.3}Mn_{1.5-x}Co_{1.5-y}O_4$ powders, XPS tests were carried out. As shown in Figure 9a, Co, Mn, Cu, O, and C were identified in the coating. According to the Co 2p spectrum in Figure 9b, the low-energy peaks (780.6 and 796.1 eV) and high-energy peaks (781.6 and 797.4 eV) in the Co $2P_{3/2}$ and $2P_{1/2}$ regions were ascribed to Co^{3+} and Co^{2+}, respectively. In addition, the peaks with binding energies of 786.6 eV and 803.6 eV were identified as the satellite peaks of Co^{2+} and Co^{3+} [22–24]. As illustrated in Figure 9c, the peaks at 641.5, 642.3, and 642.8 eV corresponded to Mn^{2+}, Mn^{3+}, and Mn^{4+}, respectively [25–27]. In Figure 9d, the peaks at 945 eV were attributed to Cu^{2+} satellites, while those at 930.8 and 933.4 eV were evidence

of the presence of Cu^+ and Cu^{2+} in the Cu $2P_{3/2}$ orbital peaks. Peaks at 953.5 and 950.6 eV can be assigned to the existence of Cu^{2+} and Cu^+, which were observed in the Cu $2P_{1/2}$ orbital [28–30]. The peaks at 530.4 eV and 531.9 eV, as shown in Figure 9e, corresponded to the oxygen-metal bond (metal = Mn, Co) and O-H bond in the spinel phase, respectively [3].
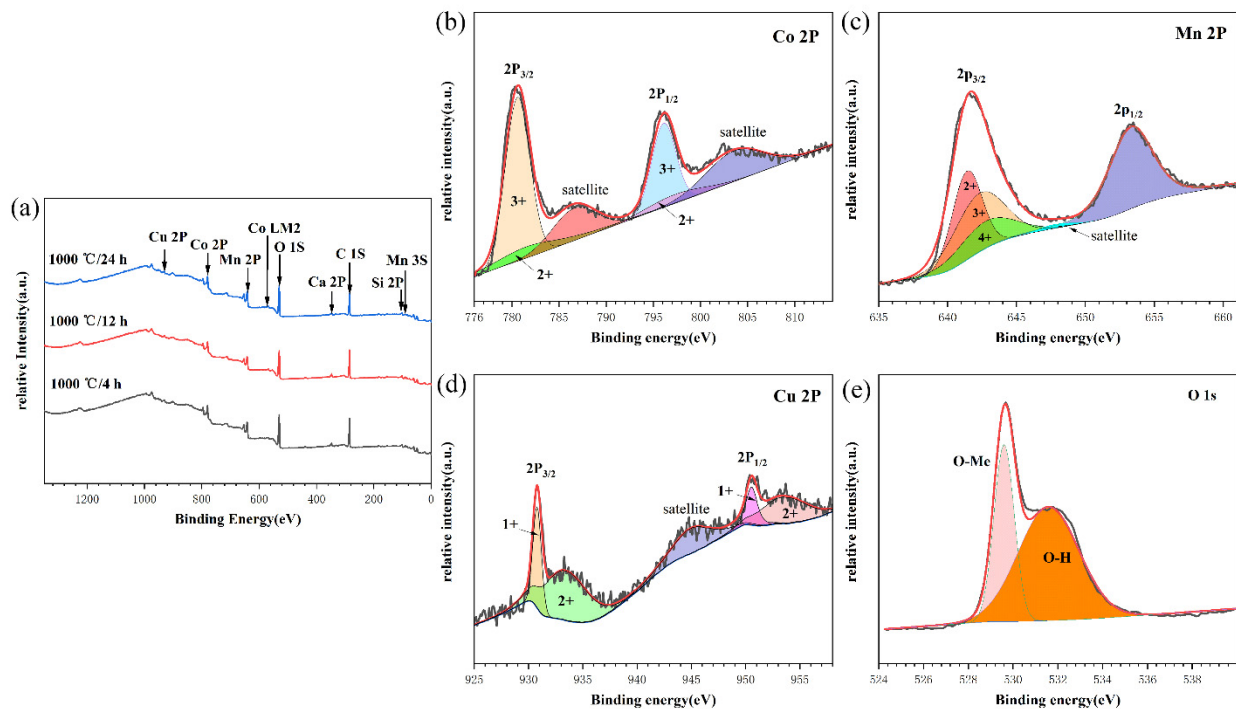
Figure 9. XPS spectra of $Cu_{0.3}Mn_{1.5-x}Co_{1.5-y}O_4$ powders sintered at 1000 °C: (**a**) survey; (**b**) Co 2P of 1000 °C/12 h sample; (**c**) Mn 2P of 1000 °C/12 h sample; (**d**) Cu 2P of 1000 °C/12 h sample; (**e**) O 1s of 1000 °C/12 h sample.

According to public reports [10,31,32], various valences exist in Mn-Co-Cu spinel. By performing a deconvolution of the XPS spectra, the relative proportion of different valence states of elements can be obtained. The relative proportion is listed in Table 3. It was found that the relative proportion of Mn^{3+} increased to 41.3% when sintered for 12 h and then decreased 33.6% after 24 h of preservation. The areal fraction of Mn^{2+} and Co^{3+} increased first and then decreased when the sintering duration increased. The increase in Mn^{3+} indicated an increase in the $CuMn_2O_4$ phase, and the decrease in Mn^{2+} and Co^{3+} was related to the decomposition of the $MnCo_2O_4$ phase. Moreover, the increase in Mn^{4+} indicated an increase in MnO_2, which diminished the conductivity of the prepared powders or coatings. According to Table 3 the powder prepared at 1000 °C and sintered for 12 h gave the most $MnCo_2O_4$ and $CuMn_2O_4$.

Table 3. Areal fractions of Mn and Co in the powders prepared under different conditions.

| Element State	Areal Fraction (%)			
	1000 °C/4 h	1000 °C/8 h	1000 °C/12 h	1000 °C/24 h
Mn^{2+}	32.3	46.2	36.7	34.2
Mn^{3+}	31.7	33.2	41.3	33.6
Mn^{4+}	36.0	20.6	22.0	32.2
Co^{2+}	23.6	20.9	17.7	26.3
Co^{3+}	76.4	79.1	82.3	73.7

3.6. Coatings Conductivity

To evaluate the doping effect, commercial $Mn_{1.5}Co_{1.5}O_4$ and $Cu_{0.3}Mn_{1.5-x}Co_{1.5-y}O_4$ powder (sintered at 1000 °C and maintained for 8 h, 12 h, and 24 h, respectively) were

sprayed on Al_2O_3 sheets with an atmospheric plasma spray; the parameters are provided in Table 1. During spraying, the spinel powder was injected into the plasma plume, the temperature of which was as high as 15,000 °C, then the injected powder was heated, melted, accelerated, and impacted on the substrate to form coatings. Deoxidization and decomposition of the spinel powder occurred during spraying; therefore, low active phases such as MnO_2 and CoO were generated and left in the coating. As a result of the very short spraying time, only a small part of the powder was decomposed, and most of the powder retained the spinel structure. Before the conductivity measurement, the sample was heated to 800 °C and maintained for 12 h to allow the densification of the coating and cure the decomposed phases. As shown in Figure 10, after the heat treatment, significant signals of $MnCo_2O_4/CuMn_2O_4$ were detected, which indicates a transference of low conductive phases to the spinel phase. For this reason, the measured coating conductivity increased with the temperature during preservation with a duration up to 50 h, as shown in Figure 11. The conductivity of the coating prepared with powder sintered for 12 h was about 51 S/cm after 47 h of preservation. For the coating prepared with powder sintered at 1000 °C for 8 h and 24 h, the conductivity was 45 S/cm and 49.2 S/cm, respectively, which are more than double that of the $Mn_{1.5}Co_{1.5}O_4$ coating, 23 S/cm after 50 h of preservation. Therefore, by applying Cu doping, the conductivity of Mn-Co spinel coatings can be significantly improved. Moreover, according to Figures 10 and 11, the coating prepared with powder sintered at 1000 °C for 8 h exhibited lower crystallinity and less spinel content, resulting in a coating conductivity lower than that of the 1000 °C/12 h and 24 h samples.
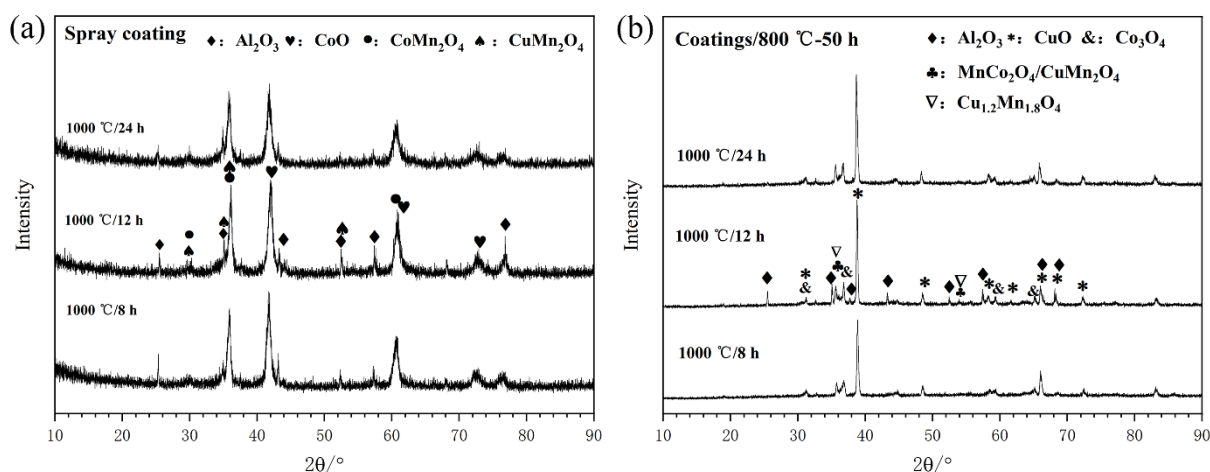

Figure 10. XRD patterns of coatings prepared with sintering powder for different times: (**a**) spray state; (**b**) coatings at 800 °C for 50 h.
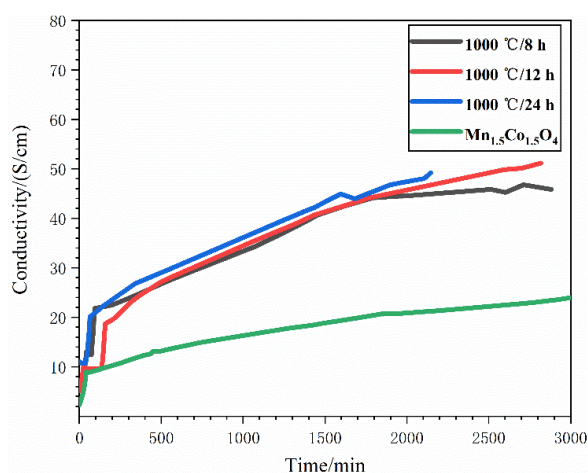
Figure 11. Coatings conductivity prepared from commercial spinel powder and $Cu_{0.3}Mn_{1.5-x}Co_{1.5-y}O_4$.

The sectional morphology and element distribution before and after the conductivity measurement of the best coating (1000 °C for 12 h) are provided in Figure 12. After the conductivity measurement, the coating was significantly densified, and no large pores or cracks were visible on the cross-section. The distribution of Mn and Co exhibited no evident variation, while Cu was found to be enriched on the coating surface. The enriched Cu on the surface was then oxidized to CuO at 800 °C, which limited the conductivity of the coatings. Despite the existence of CuO on the surface restraining the doping effect, Cu doping remains a convenient method to significantly promote the conductivity of spinel coatings for SOFC applications.
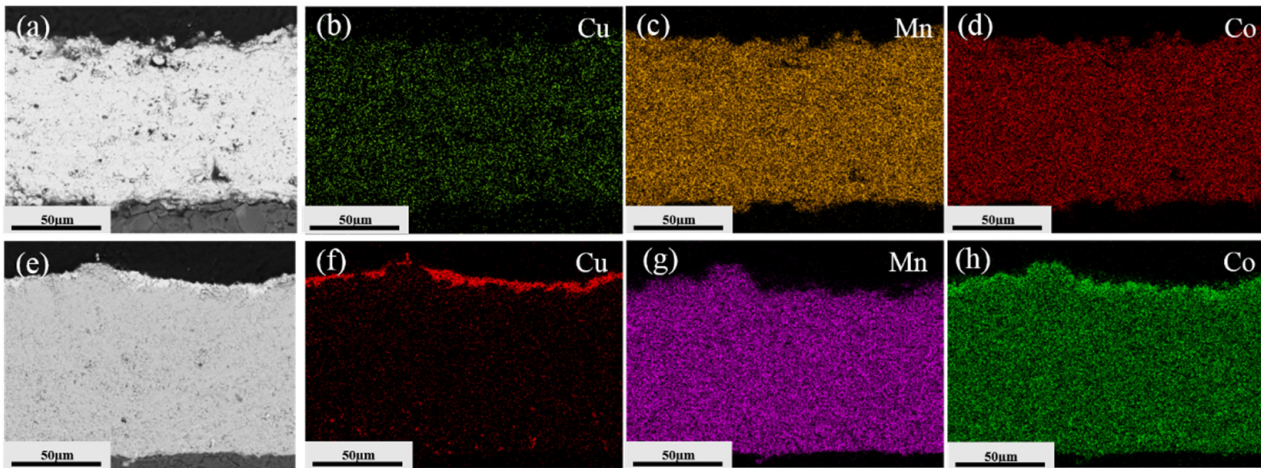
Figure 12. Morphologies and compositions of $Cu_{0.3}Mn_{1.5-x}Co_{1.5-y}O_4$ coating: (**a**–**d**) before the conductivity measurement; (**e**–**h**) after the conductivity measurement.

4. Conclusions

The powder $Cu_{\delta}Mn_{1.5-x}Co_{1.5-y}O_4$ (x + y = δ) with δ = 0.3 showed a better performance than the powder with δ = 0.1 or 0.2. The results of XRD and TG-DSC indicated that increasing the dopant amount resulted in an enhanced doping effect. With δ = 0.3, the powder had a better crystallinity and a more conductive spinel phase.

The best doping condition for $Cu_{0.3}Mn_{1.5-x}Co_{1.5-y}O_4$ powders was 1000 °C for 12 h. Under this condition, the crystallization of the spinel phase ($MnCo_2O_4$ and $Cu_xMn_{3-x}O_4$) was the best and the powder was moderately dense. The dopant Cu was found to be evenly distributed in the powders. The $Cu_xMn_{3-x}O_4$ (x = 1, 1.2, 1.4 or 1.5) was found to be mainly composed of $CuMn_2O_4$ and was sufficiently stable at elevated temperatures. According to the XPS results, the powder prepared at 1000 °C for 12 h consisted of the most $MnCo_2O_4$ and $CuMn_2O_4$. When the preservation stage was conducted at 1000 °C with a duration of less than 12 h or more than 12 h, less $MnCo_2O_4$ and $Cu_xMn_{3-x}O_4$ phases were detected.

Coatings were prepared with doped powders using an atmospheric plasma spray. After preservation at 800 °C for a duration of up to 50 h, the measured conductivity of the prepared coatings reached 45 S/cm, 51 S/cm, and 49.2 S/cm, respectively, i.e., two times more than that of the $Mn_{1.5}Co_{1.5}O_4$ coating (23 S/cm). Although Cu was enriched on the coating surface after the conductivity measurement, Cu-doping is still an effective method to improve the conductivity of spinel coatings used for interconnect protection in SOFC.

Author Contributions: Formal analysis, Z.J.; investigation, Z.J. and C.S.; methodology, K.W. and T.L.; project administration, M.L.; resources, C.D. (Changguang Deng); supervision, C.D. (Chunming Deng) and Y.D.; writing—original draft, Z.J.; writing—review and editing, T.L. and C.Y. All authors have read and agreed to the published version of the manuscript.

Institutional Review Board Statement: Not applicable.

Informed Consent Statement: Not applicable.

Data Availability Statement: The data presented in this study are available on request from the corresponding author.

References

1. Shong, W.J.; Liu, C.K.; Chen, C.Y.; Peng, C.C.; Tu, H.J.; Fey, G.T.K.; Lee, R.Y.; Kao, H.M. Effects of lanthanum-based perovskite coatings on the formation of oxide scale for ferritic SOFC interconnect. *Mater. Chem. Phys.* **2011**, *127*, 45–50. [CrossRef]
2. Stanislowski, M.; Froitzheim, J.; Niewolak, L.; Quadakkers, W.J.; Hilpert, K.; Markus, T.; Singheiser, L. Reduction of chromium vaporization from SOFC interconnectors by highly effective coatings. *J. Power Sources* **2007**, *164*, 578–589. [CrossRef]
3. Zou, J.; Song, C.; Wen, K.; Liu, T.; Deng, C.; Liu, M.; Yang, C. The Microstructure and Conductivity Evolution of Plasma-Sprayed (Mn, Co)$_3$O$_4$ Spinel Coatings during Conductivity Measurements at Elevated Temperature. *Coatings* **2021**, *11*, 533. [CrossRef]
4. Grünwald, N.; Sohn, Y.J.; Yin, X.; Menzler, N.H.; Guillon, O.; Vaßen, R. Microstructure and phase evolution of atmospheric plasma sprayed Mn-Co-Fe oxide protection layers for solid oxide fuel cells. *J. Eur. Ceram. Soc.* **2019**, *39*, 449–460. [CrossRef]
5. Xin, X.; Zhu, Q.; Liu, Y. Conductive protective coating with heat oxygen-resistance for solid oxide fuel cell (SOFC) alloy interconnect. *Surf. Technol.* **2019**, *48*, 22–29. [CrossRef]
6. Jiang, S.P. Development of lanthanum strontium cobalt ferrite perovskite electrodes of solid oxide fuel cells-A review. *Int. J. Hydrogen Energy.* **2019**, *44*, 7448–7493. [CrossRef]
7. Tan, K.H.; Rahman, H.A.; Taib, H. Coating layer and influence of transition metal for ferritic stainless steel interconnector solid oxide fuel cell: A review. *Int. J. Hydrogen Energy* **2019**, *44*, 30591–30605. [CrossRef]
8. Mah, J.C.W.; Muchtar, A.; Somalu, M.R.; Ghazali, M.J. Metallic interconnects for solid oxide fuel cell: A review on protective coating and deposition techniques. *Int. J. Hydrogen Energy* **2017**, *42*, 9219–9229. [CrossRef]
9. Waluyo, N.S.; Park, S.S.; Song, R.H.; Lee, S.-B.; Lim, T.-H.; Hong, J.-E.; Ryu, K.H.; Bin Im, W.; Lee, J.-W. Protective coating based on manganese–copper oxide for solid oxide fuel cell interconnects: Plasma spray coating and performance evaluation. *Ceram. Int.* **2018**, *44*, 11576–11581. [CrossRef]
10. Talic, B.; Hendriksen, P.V.; Wiik, K.; Lein, H.L. Thermal expansion and electrical conductivity of Fe and Cu doped MnCo$_2$O$_4$ spinel. *Solid State Ion.* **2018**, *326*, 90–99. [CrossRef]
11. Talic, B.; Hendriksen, P.V.; Wiik, K.; Lein, H.L. Diffusion couple study of the interaction between Cr$_2$O$_3$ and MnCo$_2$O$_4$ doped with Fe and Cu. *Solid State Ion.* **2019**, *332*, 16–24. [CrossRef]
12. Puranen, J.; Pihlatie, M.; Lagerbom, J.; Bolelli, G.; Laakso, J.; Hyvärinen, L.; Kylmälahti, M.; Himanen, O.; Kiviaho, J.; Lusvarghi, L.; et al. Post-mortem evaluation of oxidized atmospheric plasma sprayed Mn–Co–Fe oxide spinel coatings on SOFC interconnectors. *Int. J. Hydrogen Energy* **2014**, *39*, 17284–17294. [CrossRef]
13. Liu, Y.; Fergus, J.W.; Wang, K.; Cruz, C.D. Crystal Structure, Chemical Stabilities and Electrical Conductivity of Fe-Doped Manganese Cobalt Spinel Oxides for SOFC Interconnect Coatings. *J. Electrochem. Soc.* **2013**, *160*, F1316–F1321. [CrossRef]
14. Zhu, J.H.; Lewis, M.J.; Du, S.W.; Li, Y. CeO$_2$-doped (Co,Mn)$_3$O$_4$ coatings for protecting solid oxide fuel cell interconnect alloys. *Thin Solid Films* **2015**, *596*, 179–184. [CrossRef]
15. Tseng, H.P.; Yung, T.Y.; Liu, C.K.; Cheng, Y.-N.; Lee, R.-Y. Oxidation characteristics and electrical properties of La- or Ce-doped MnCo$_2$O$_4$ as protective layer on SUS441 for metallic interconnects in solid oxide fuel cells. *Int. J. Hydrogen Energy* **2020**, *45*, 12555–12564. [CrossRef]
16. Gavrilov, N.V.; Ivanov, V.V.; Kamenetskikh, A.S.; Nikonov, A. Investigations of Mn–Co–O and Mn–Co–Y–O coatings deposited by the magnetron sputtering on ferritic stainless steels. *Surf. Coat. Technol.* **2011**, *206*, 1252–1258. [CrossRef]
17. Brylewski, T.; Kruk, A.; Bobruk, M.; Adamczyk, A.; Partyka, J.; Rutkowski, P. Structure and electrical properties of Cu-doped Mn-Co-O spinel prepared via soft chemistry and its application in intermediate-temperature solid oxide fuel cell interconnects. *J. Power Sources* **2016**, *333*, 145–155. [CrossRef]
18. Xu, Y.; Wen, Z.; Wang, S.; Wen, T. Cu doped Mn–Co spinel protective coating on ferritic stainless steels for SOFC interconnect applications. *Solid State Ion.* **2011**, *192*, 561–564. [CrossRef]
19. Sabato, A.G.; Molin, S.; Javed, H.; Zanchi, E.; Boccaccini, A.R.; Smeacetto, F. In-situ Cu-doped MnCo-spinel coatings for solid oxide cell interconnects processed by electrophoretic deposition. *Ceram. Int.* **2019**, *45*, 19148–19157. [CrossRef]

20. Wei, P.; Bieringer, M.; Cranswick, L.M.D.; Petric, A. In situ high-temperature X-ray and neutron diffraction of Cu–Mn oxide phases. *J. Mater. Sci.* **2010**, *45*, 1056–1064. [CrossRef]

21. Masi, A.; Bellusci, M.; McPhail, S.J.; Padella, F.; Reale, P.; Hong, J.-E.; Steinberger-Wilckens, R.; Carlini, M. Cu-Mn-Co oxides as protective materials in SOFC technology: The effect of chemical composition on mechanochemical synthesis, sintering behaviour, thermal expansion and electrical conductivity. *J. Eur. Ceram. Soc.* **2017**, *37*, 661–669. [CrossRef]

22. Waskowska, A.; Gerward, L.; Olsen, J.S.; Steenstrup, S.; Talik, E. $CuMn_2O_4$: Properties and the high-pressure induced Jahn-Teller phase transition. *J. Phys. Condens. Matter* **2001**, *13*, 2549–2562. [CrossRef]

23. Hu, Y.Z.; Su, Y.T.; Li, C.X.; Li, C.-J.; Yang, G.-J. Dense $Mn_{1.5}Co_{1.5}O_4$ coatings with excellent long-term stability and electrical performance under the SOFC cathode environment. *Appl. Surf. Sci.* **2020**, *499*, 143726. [CrossRef]

24. Fan, L.Q.; Huang, J.L.; Wang, Y.L.; Geng, C.-L.; Sun, S.-J.; Huang, Y.-F.; Lin, J.-M.; Wu, J.-H. TiO_2 nanotubes supported ultrafine $MnCo_2O_4$ nanoparticles as a superior-performance anode for lithium-ion capacitors. *Int. J. Hydrogen Energy* **2021**, *46*, 35330–35341. [CrossRef]

25. Li, J.; Xiong, S.; Li, X.; Qian, Y. A facile route to synthesize multiporous $MnCo_2O_4$ and $CoMn_2O_4$ spinel quasi-hollow spheres with improved lithium storage properties. *Nanoscale* **2013**, *5*, 2045–2054. [CrossRef]

26. Umezawa, Y.; Reilley, C.N. Effect of argon ion bombardment on metal complexes and oxides studied by x-ray photoelectron spectroscopy. *Anal. Chem.* **1978**, *50*, 1290–1295. [CrossRef]

27. Vepřek, S.; Cocke, D.L.; Kehl, S.; Oswald, H.R. Mechanism of the deactivation of Hopcalite catalysts studied by XPS, ISS, and other techniques. *J. Catal.* **1986**, *100*, 250–263. [CrossRef]

28. Liu, Y.; Song, Z.; Wang, W.; Wang, Z.; Zhang, Y.; Liu, C.; Wang, Y.; Li, A.; Xu, B.; Qi, F. A $CuMn_2O_4/g-C_3N_4$ catalytic ozonation membrane reactor used for water purification: Membrane fabrication and performance evaluation. *Sep. Purif. Technol.* **2021**, *265*, 118268. [CrossRef]

29. Fang, R.; Liu, F.; Liu, J.; Li, Y. Experimental and theoretical insights into the reaction mechanism of spinel $CuMn_2O_4$ with CO in chemical-looping combustion. *Appl. Surf. Sci.* **2021**, *561*, 150065. [CrossRef]

30. Thaheem, I.; Joh, D.W.; Noh, T.; Lee, K.T. Highly conductive and stable $Mn_{1.35}Co_{1.35}Cu_{0.2}Y_{0.1}O_4$ spinel protective coating on commercial ferritic stainless steels for intermediate-temperature solid oxide fuel cell interconnect applications. *Int. J. Hydrogen Energy* **2019**, *44*, 4293–4303. [CrossRef]

31. Bobruk, M.; Durczak, K.; Dąbek, J.; Dąbek, J.; Brylewski, T. Structure and Electrical Properties of Mn-Cu-O Spinels. *J. Mater. Eng. Perform.* **2017**, *26*, 1598–1604. [CrossRef]

32. Joshi, S.; Petric, A. Nickel substituted $CuMn_2O_4$ spinel coatings for solid oxide fuel cell interconnects. *Int. J. Hydrogen Energy* **2017**, *42*, 5584–5589. [CrossRef]